Hindawi Publishing Corporation
Advances in Materials Science and Engineering
Volume 2016, Article ID 6942696, 10 pages
http://dx.doi.org/10.1155/2016/6942696

Research Article

Influences by Air Voids on the Low-Temperature Cracking Property of Dense-Graded Asphalt Concrete Based on Micromechanical Modeling

Tao Ma,[1] Yao Zhang,[1] Hao Wang,[2] Xiaoming Huang,[1] and Yongli Zhao[1]

[1]*School of Transportation, Southeast University, Nanjing 210096, China*
[2]*Department of Civil and Environmental Engineering, Rutgers, The State University of New Jersey, Piscataway, NJ 08854, USA*

Correspondence should be addressed to Tao Ma; matao@seu.edu.cn

Received 25 June 2016; Accepted 22 September 2016

Academic Editor: Ying Li

This study characterized the impacts of air voids on the low-temperature cracking behavior of dense-graded asphalt concrete. Virtual low-temperature bending beam test for dense-graded asphalt concrete was built and executed by discrete element method and PFC3D (particle flow code in three dimensions). Virtual tests were applied to analyze the impacts by content, distribution, and size of air voids on the low-temperature properties of dense-graded asphalt concrete. The results revealed that higher air void content results in worse low-temperature property of dense-graded asphalt concrete, especially when the air void content exceeds the designed air content; even with the same designed air void content, different distributing condition of air voids within asphalt concrete leads to different low-temperature properties of asphalt concrete, especially when the air void content in the central-lower part of testing sample varies. Bigger size of single air void which tends to form interconnected air voids within asphalt concrete has more harmful impacts on the low-temperature properties of asphalt concrete. Thus, to achieve satisfied low-temperature properties of dense-graded asphalt concrete, it is critical to ensure the designed air void content, improve the distribution of air voids, and reduce the interconnected air voids for dense-graded asphalt concrete.

1. Introduction

Low-temperature cracking is one of the main diseases of asphalt pavement especially in cold weather. Since asphalt concrete is typical heterogeneous composite materials, the composition ratios of different constituents within asphalt concrete and their microstructure distribution have important influences on the cracking behavior of asphalt concrete [1, 2]. However, laboratory tests cannot fully evaluate the influences by different constituents of asphalt concrete on its cracking behavior [3]. Although finite element method can well depict the cracking behavior of asphalt concrete, it still has difficulties to characterize the heterogeneity of asphalt concrete and depict the microstructure of different constituents of asphalt concrete [4–8]. The discrete element method proposed by Cundall can evaluate the interacting behavior within discrete particles by characterizing the translational and rational movements of different particles based on Newton's second law of motion and a finite difference scheme [9, 10]. It provides a more promising way to model and describe the heterogeneous microstructure and micromechanical behavior of asphalt concrete.

After contact-bonding relationships for asphalt concrete were built, DEM has been extensively used to characterize the performances of asphalt concrete. Although many different discrete element software have been developed, the particle flow code in two and three dimensions (PFC2D/3D) was used most popularly for asphalt concrete analysis due to its good modeling productivity and flexible capacity to characterize the moving behavior and interaction between the different ingredients of asphalt concrete [11]. Abbas et al. and Liu and Dai conducted micromechanical modeling for asphalt concrete and analyzed the viscoelastic behavior of asphalt concrete based on discrete element method [12, 13]. Collop et al. performed uniaxial compressive creep test simulation for asphalt concrete based on elastic contacting model [14].

Table 1: Mix design of AC13 and asphalt mortar.

AC13	Sieving size/mm	16	13.2	9.5	4.75	2.36	1.18	0.6	0.3	0.15	0.075
	Passing ratio/%	100	95	79.7	49.8	37.6	26.4	17.1	9.8	7.2	6.6
	Asphalt content/%	4.9%									
Asphalt mortar	Sieving size/mm	/	/	/	/	2.36	1.18	0.6	0.3	0.15	0.075
	Passing ratio/%	/	/	/	/	100	70.2	45.4	26.1	19.1	17.6
	Asphalt content/%	11.0%									

Based on the combination of DEM and image processing technology, You et al. built three-dimensional DEM model of asphalt concrete and simulated the dynamic modulus test of asphalt concrete to predict the compressible dynamic moduli of asphalt concrete [15] and Khattak and Roussel and Khattak et al. developed a two-dimensional DEM model of asphalt concrete to analyze the strength and dynamic modulus of asphalt concrete under indirect tension mode [16, 17]. Based on random modeling algorithm for asphalt concrete, Zhang et al. and Hou et al. investigated the micromechanical response of asphalt concrete under loading pressure and analyzed the rutting property and mechanism of asphalt concrete [18, 19]. Buttlar et al. and Kim et al. investigated the tension failure behavior and fracture energy by simulating the single-edge notched beam test and disk-shaped compact tension test [20, 21]. Kim and Buttlar studied the discrete fracture modeling for asphalt concrete and investigated the fracture behavior of asphalt concrete [22, 23]. Yang et al. simulated the bending beam fracture test by adopting discrete element method and analyzed the healing property of asphalt concrete by using bond healing model [24]. Chen et al. investigated both the dynamic behavior and the fracture behavior of asphalt concrete by simulating the creep test and splitting test of asphalt concrete [25, 26].

However, few researches were performed to evaluate and analyze the low-temperature cracking behavior based on three-dimensional discrete element modeling and the impacts by air voids on the low-temperature properties of asphalt concrete. This study focused on the impacts of different parameters of air voids on the low-temperature properties of dense-graded asphalt concrete. DEM and PFC3D were used to build three-dimensional digital sample and virtual low-temperature bending beam test for dense-graded asphalt concrete based on laboratory tests. And the influences of air void content, distribution of air voids, and size of single air void on the low-temperature properties of asphalt concrete were analyzed.

2. Materials and Experimental Test

2.1. Materials. A 13 mm dense-graded asphalt concrete (AC13) with nominal maximum aggregate size of 13.2 mm, which was widely used as the wearing course in China, was prepared for laboratory test and micromechanical modeling. The mix design of AC13 satisfied the specifications set forth by Chinese Ministry of Transportation and is shown in Table 1. If all of the aggregates especially the fine aggregates and mineral fillers were considered during micromechanical modeling for asphalt concrete, it is too time-consuming to generate virtual sample and conduct the virtual test during PFC3D. Thus, to facilitate micromechanical modeling in PFC3D, asphalt concrete was considered as a three-phase composition that consisted of three ingredients which are air voids, asphalt mortar composed of asphalt binder and fine aggregates passing 2.36 mm sieving size, and coarse aggregates retained on 2.36 mm sieving size.

2.2. Experimental Tests. The low-temperature three-point bending beam test was performed for AC13 by Universal Testing Machine (UTM). The testing temperature was −10°C. And loading was applied by cylindrical pressure bar with diameter of 2 cm on the span center of the beam sample with dimensions of 250 × 30 × 35 mm^3 (length × width × height) at loading speed of 50 mm/min until the beam was ruptured. Based on the rupture load and the rupture displacement at the span center of beam sample immediately after the sample was ruptured, the fracture tensile stress, fracture tensile strain, and fracture strain energy density can be obtained and recorded. The low-temperature splitting test was conducted at −10°C for asphalt mortar. During the splitting test, loading was applied on the cylindrical sample with height of 63.5 mm and diameter of 101.6 mm at loading speed of 50 mm/min until the sample was split to get the splitting tensile stress and splitting tensile modulus for mortar sample. Figure 1 shows the test samples for the low-temperature three-point bending beam test and low-temperature splitting test, respectively.

3. Discrete Element Modeling for Virtual Test

3.1. Micromechanical Models and Parameters. During PFC3D modeling, the microstructure of asphalt concrete was modeled as a three-ingredient system (coarse aggregates, asphalt mortar, and air voids) and different contact models were used to describe the micromechanical behavior of different ingredients. Based on PFC3D manual [27], the contact models at different contacts within asphalt concrete are summarized in Table 2.

The micromechanical parameters for different contact models can be determined by the macromechanical properties of coarse aggregates and asphalt mortar [27], as shown in the following:

$$k_n = 4ER,$$

$$k_s = \frac{2E}{1+\nu}R,$$

$$\mu_c = \mu_a,$$

Table 2: Contact models at different contacts within asphalt concrete.

Contacts	Contact models
Between aggregates	Contact-stiffness model and slip model
Within asphalt mortar	Contact-stiffness model and contact-bonding model
Between aggregate and mortar	Contact-stiffness model and contact-bonding model

(a) (b)

Figure 1: Test samples during laboratory tests: (a) low-temperature bending beam test; (b) low-temperature splitting test.

$$
\begin{aligned}
k_n' &= 4E'R, \\
k_s' &= \frac{2E'}{1+\nu'}R, \\
\varphi_n &= 4R^2\sigma_t, \\
k_n'' &= \frac{4EE'}{E+E'}R, \\
k_s'' &= \frac{4EE'}{(1+\nu')E + 2(1+\nu)E'}R, \\
\varphi_n' &= \varphi_n,
\end{aligned}
\tag{1}
$$

where k_n, k_s, and μ_c are the normal stiffness, shear stiffness, and friction coefficient at contacts between aggregates; k_n', k_s', and φ_n are the normal stiffness, shear stiffness, and maximum tensile force at contacts within asphalt mortar; k_n'', k_s'', and φ_n' are the normal stiffness, shear stiffness, and maximum tensile force at contacts within asphalt mortar; R is the radius of the discrete ball element for aggregate and asphalt mortar which is 1 mm in this study; E, ν, and μ_a are the elastic modulus, Poisson ratio, and friction coefficient of aggregates; and E' and σ_t are the tensile modulus and strength from splitting test of asphalt mortar.

Based on previous research [15, 26], the elastic modulus and friction coefficient of coarse aggregates are presented in Table 3. Based on splitting tests of asphalt mortar, the tensile stress and modulus of asphalt mortar are also summarized in Table 3. According to (1), the micromechanical modeling parameters at different contacts within asphalt concrete are determined and presented in Table 4.

Table 3: Macroscale mechanical parameters for aggregates and asphalt mortar.

E/GPa	μ_a	σ_t/MPa	E'/MPa
55.5	0.5	5.6	2439

3.2. Micromechanical Modeling of Virtual Test. During micromechanical modeling by PFC3D, asphalt mortar was modeled by discrete ball elements with the same size, and air voids were considered to be distributed within asphalt mortar randomly and simulated by removing elements of asphalt mortar randomly to meet the designed air void content of asphalt concrete. However, PFC3D cannot generate irregular elements directly; thus, a user-defined modeling algorithm was performed in PFC3D to get polyhedrons with irregular shapes to simulate coarse aggregates. Based on the previous assumptions and the testing conditions of laboratory low-temperature bending beam test, as shown in Figure 2, a micromechanical modeling procedure was proposed to build virtual low-temperature bending beam test. Figure 3 shows the critical generation process during PFC3D modeling for virtual low-temperature bending beam test.

4. Results and Discussion

4.1. Validity Verification of Virtual Test. The laboratory bending beam test was conducted to verify the reliability of the virtual bending beam test. The failure sample from the

Table 4: Micromechanical modeling parameters at different contacts.

k_n/(N/m)	k_s/(N/m)	μ_c	k_n'/(N/m)	k_s'/(N/m)	φ_n/N	k_n''/(N/m)	k_s''/(N/m)	φ_n'/N
2.22×10^8	8.88×10^7	0.5	4.88×10^6	1.96×10^6	22.4	9.35×10^6	6.06×10^6	22.4

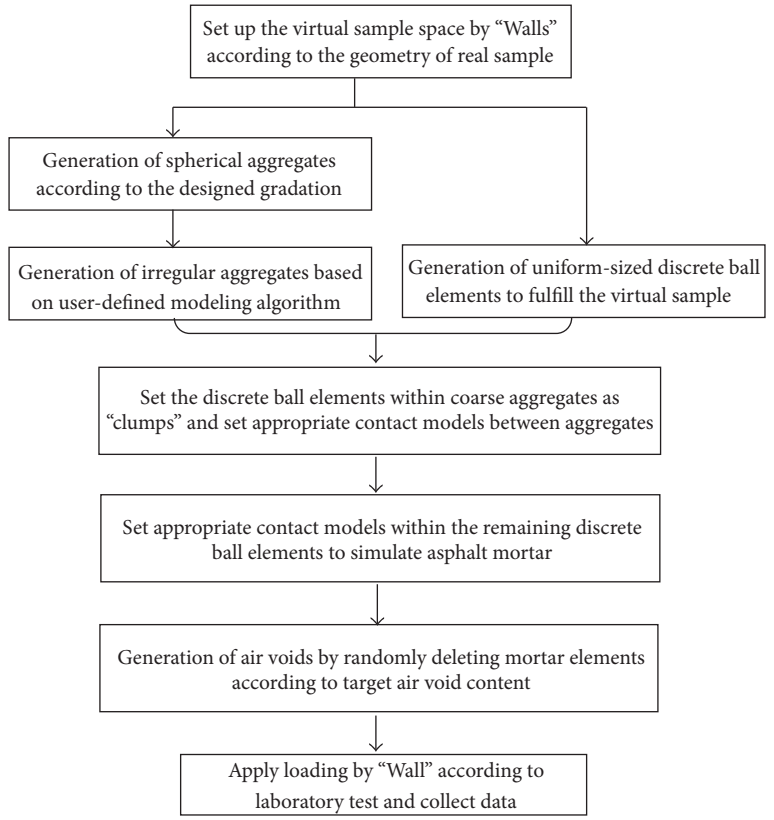

Figure 2: PFC3D modeling process for virtual bending beam test.

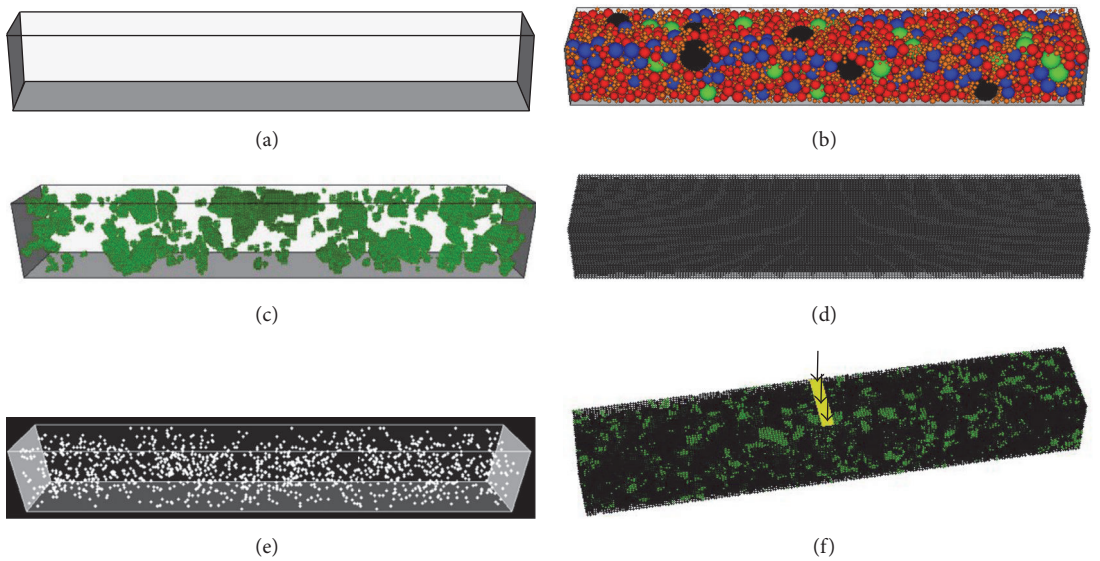

Figure 3: Illustration of modeling procedure: (a) generation of virtual sample space; (b) generation of graded spherical aggregates; (c) generation of irregular aggregates; (d) generation of asphalt mortar; (e) generation of air voids; (f) loading.

Figure 4: Failure sample from laboratory bending beam test.

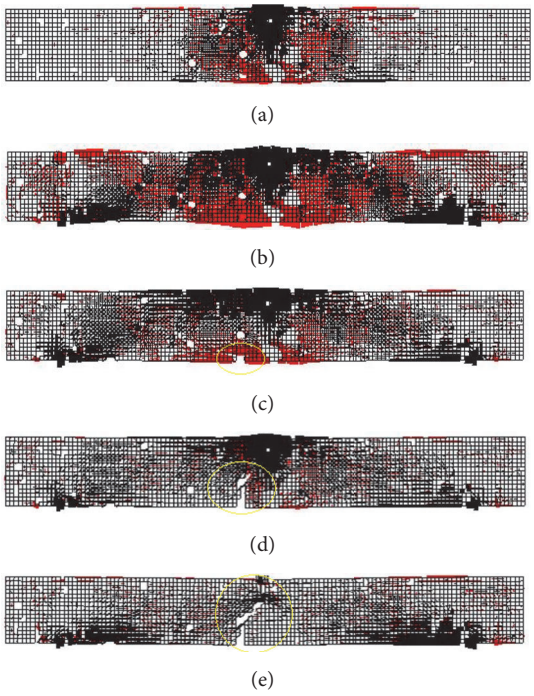

Figure 5: Illustration of different stages during virtual test: (a) initial loading; (b) maximum loading; (c) initiation of cracking; (d) extension of cracking; (e) penetration of cracking.

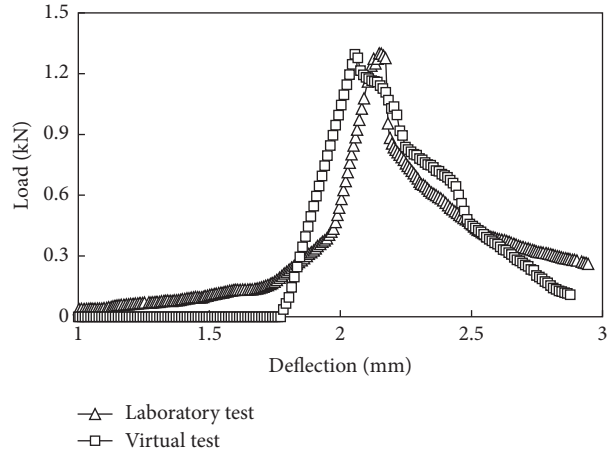

Figure 6: Testing results from laboratory test and virtual test.

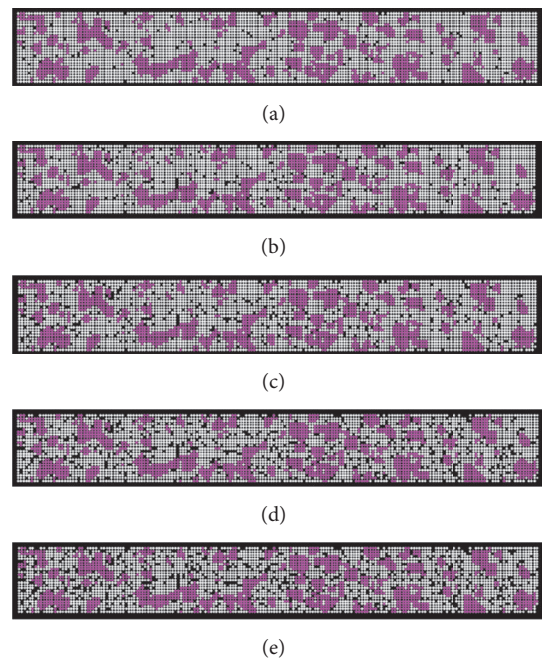

Figure 7: Cross sections of virtual sample with different air void contents: (a) 2%; (b) 4%; (c) 6%; (d) 8%; (e) 10%.

laboratory test is shown in Figure 4 while Figure 5 illustrates the different testing stages during virtual test. It can be seen that the virtual test can capture the developing process of cracking failure which is very similar to the cracking failure of the laboratory test. Figure 6 shows the test curves from laboratory test and virtual test. It can be seen that the testing curve of virtual test is similar to the testing curve of laboratory test. It proves the validity of using virtual bending beam test to predict the low-temperature property of asphalt concrete.

4.2. Effects by Content of Air Voids on Low-Temperature Property. Based on the built modeling process, as shown in Figure 7, beam samples with different contents of air voids (2%, 4%, 6%, 8%, and 10%) were built for virtual low-temperature bending beam test to analyze the influences by air void content on the low-temperature properties of asphalt concrete. The changing of tensile failure strength and failure strain with variation of air void contents are shown in Figure 8. It can be seen that all of the three indices including failure strength, failure strain, and strain energy density decrease with the air void contents increasing, especially for the strain energy density. It indicates that the low-temperature property of asphalt concrete gets worse with its air void content growing. When the air void content exceeds 6% especially, the degradation of low-temperature property becomes more serious. It well confirms with the idea that the common mix design of asphalt concrete tends to keep the target air void content lower than 6%.

4.3. Effects by Air Voids Distribution on Low-Temperature Property. During the virtual bending beam test, while the total content of air voids of test sample was kept as 4%, the nonuniform vertical distribution and nonuniform horizontal distribution of air voids in test sample were simulated, respectively, as shown in Figures 9 and 10. In Figure 9, along the vertical direction, the samples were cut apart into two parts with equal volume. Five different air void content distributions, which are 8% in the upper part and 0% in the

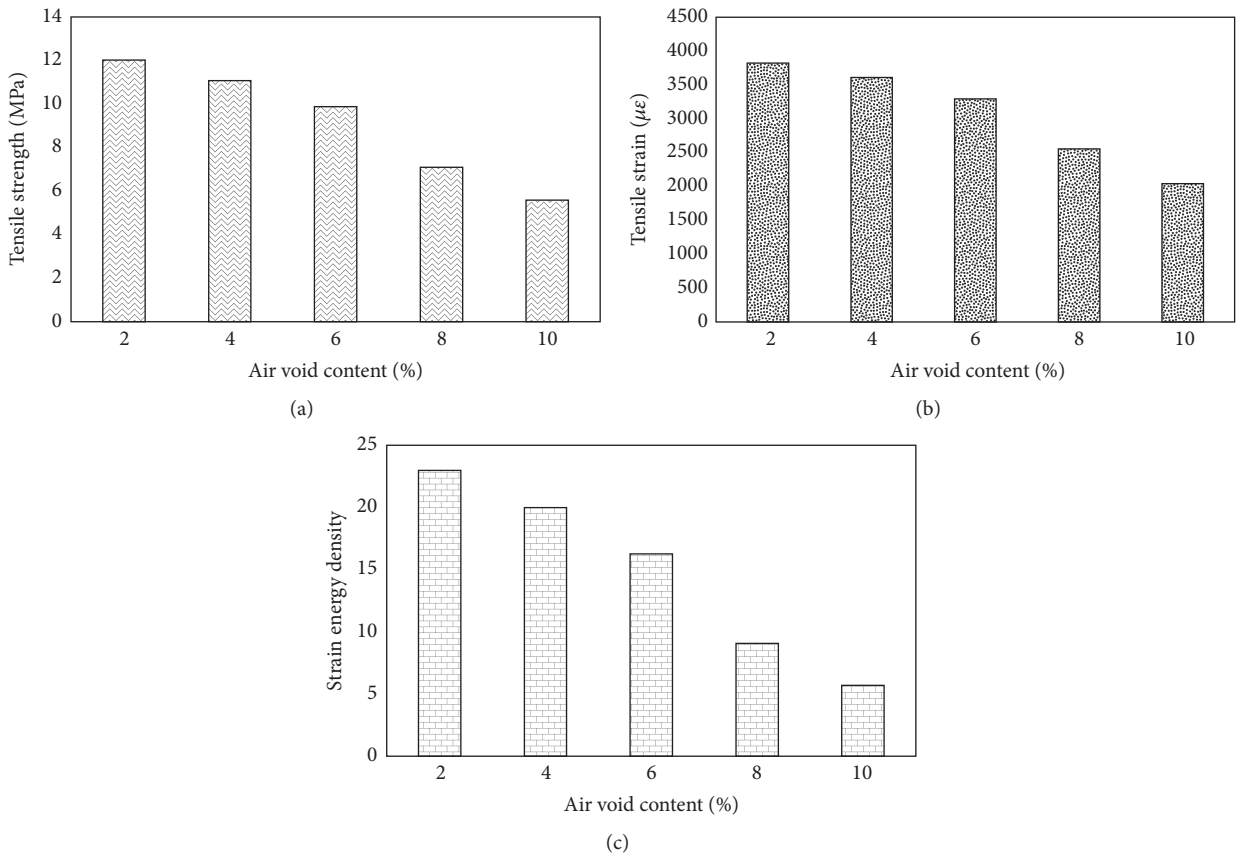

Figure 8: Testing results at different air void contents: (a) tensile failure strength; (b) tensile failure strain; (c) strain energy density.

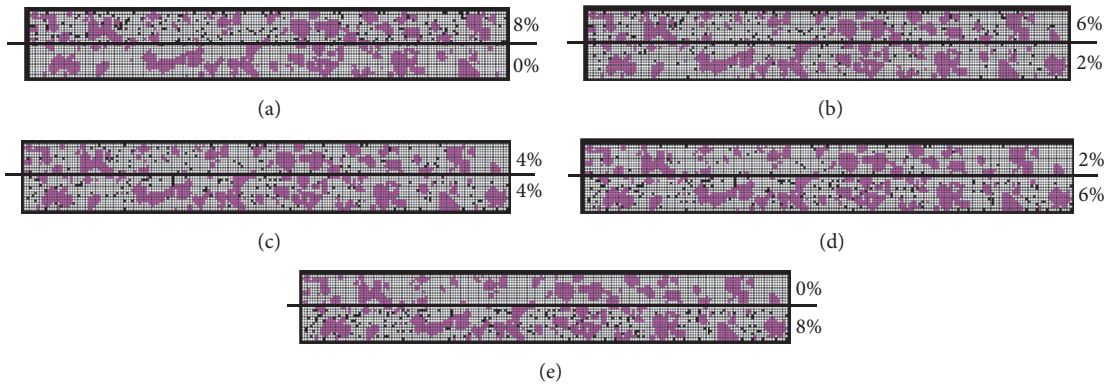

Figure 9: Vertical distribution of air voids: (a) V8/0; (b) V6/2; (c) V4/4; (d) V2/6; (e) V0/8.

lower part (V8/0), 6% in the upper part and 2% in the lower part (V6/2), 4% in the upper part and 4% in the lower part (V4/4), 2% in the upper part and 6% in the lower part (V2/6), and 0% in the upper part and 8% in the lower part (V0/8), were generated. In Figure 10, along the horizontal direction, the samples were cut apart into three parts with the same volume. Six different air void content distributions, which are 0% in the side parts and 12% in the middle parts (H0/12/0), 1% in the side parts and 0% in the middle part (H1/10/1), 2% in the side parts and 8% in the middle part (H2/8/2), 4% in all of the three parts (H4/4/4), 5% in the side parts and 2% in the middle part (H5/2/5), and 6% in the side parts and 0% in the middle part (H6/0/6), were considered.

Figures 11 and 12 show the testing results of asphalt concrete samples with different nonuniform air voids distribution. It is indicated that different air voids distributions within the samples result in different low-temperature properties. From Figure 11(a), it can be seen that the failure strength increases with the air void content of bottom lower part declining. From Figures 11(b) and 11(c), it is shown that

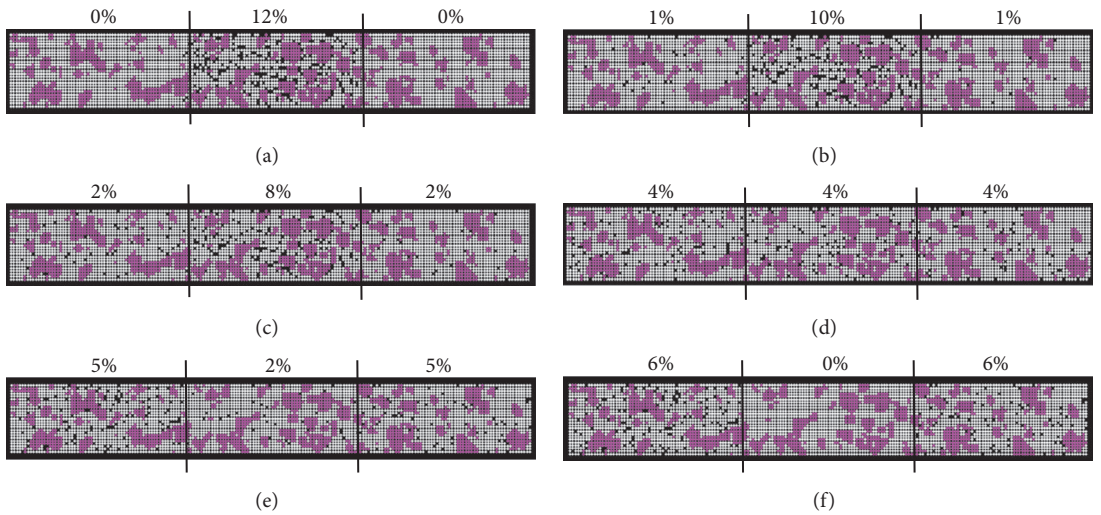

Figure 10: Horizontal distribution of air voids: (f) H-0/12/0; (e) H-1/10/1; (d) H-2/8/2; (c) H-4/4/4; (b) H-5/2/5; (a) H-6/0/6.

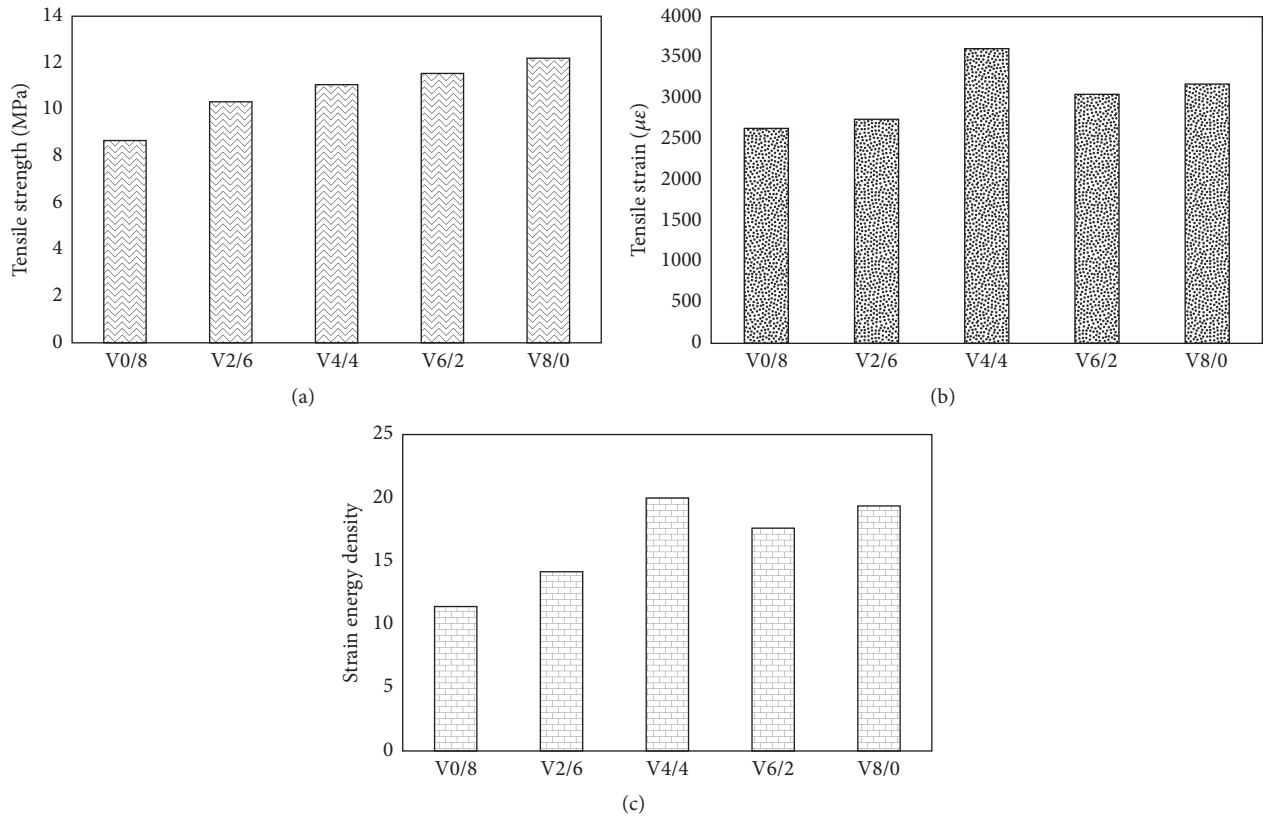

Figure 11: Testing results under different nonuniform vertical distribution of air voids: (a) tensile failure strength; (b) tensile failure strain; (c) strain energy density.

the sample with uniform distribution of air voids has the biggest failure strain and strain energy density; besides that both the failure strain and strain energy density increase with the air void content of lower part declining. It indicates that the air void content variation of lower part has more influences on the low-temperature property than that of the upper part. From Figure 12, it is shown that all of the three indices decrease with the air void content of middle part growing. When the air void content of middle part exceeds 6% especially, the degradation of all of the three indices becomes more sharp. Since the loading was applied in the center of the middle part, it confirms well with the previous

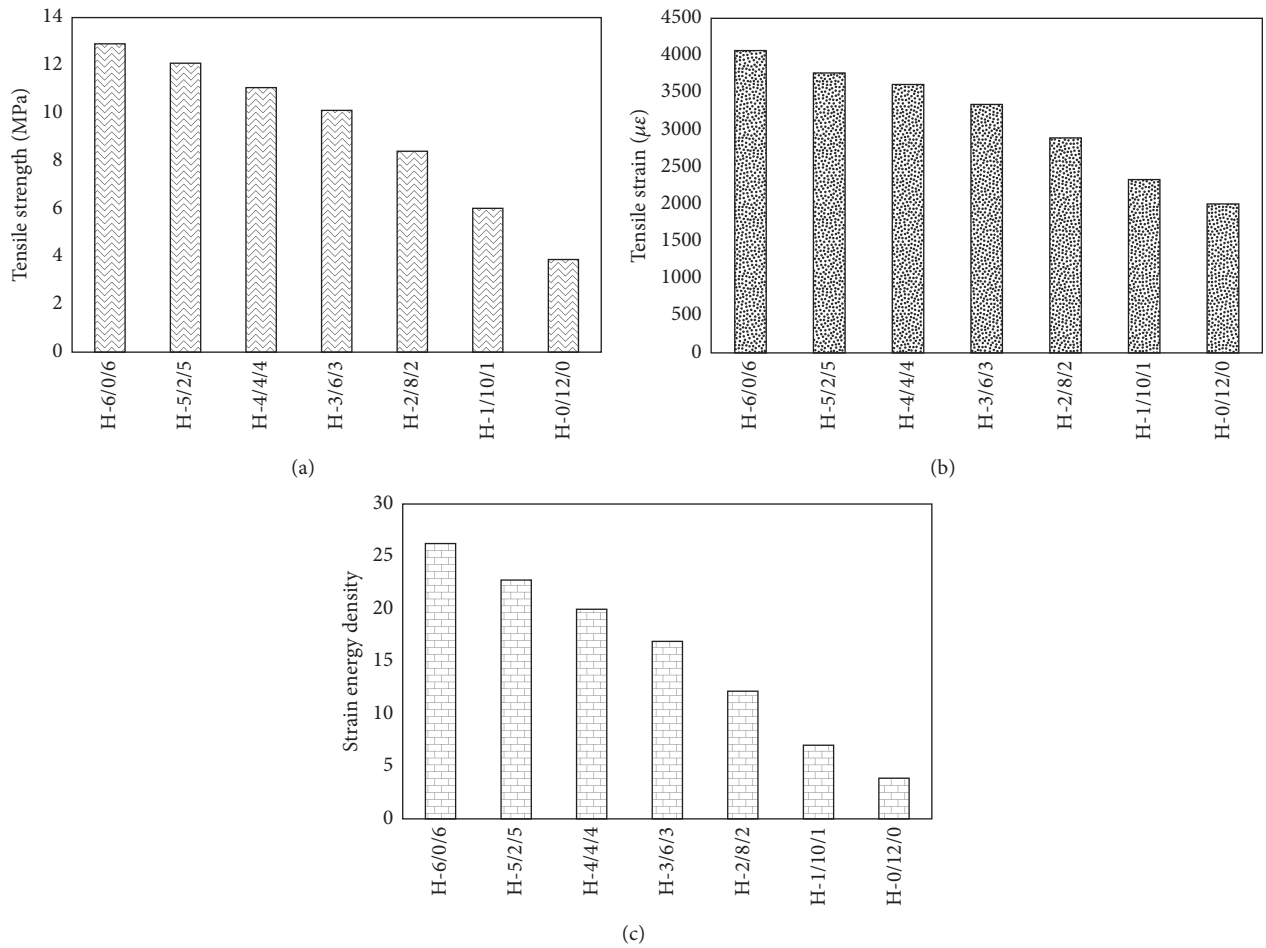

Figure 12: Testing results under different nonuniform horizontal distribution of air voids: (a) tensile failure strength; (b) tensile failure strain; (c) strain energy density.

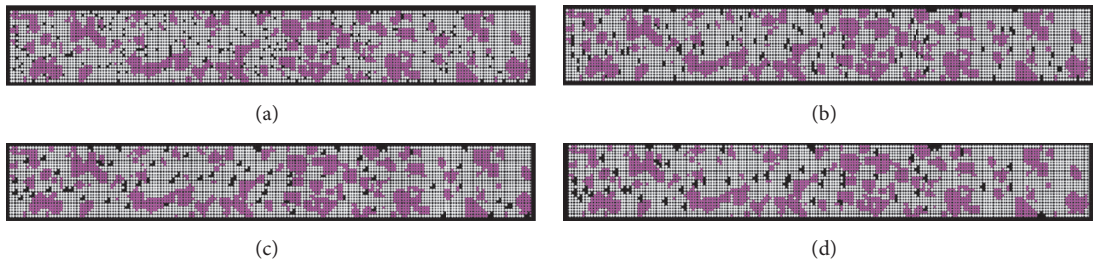

Figure 13: Samples with different sizes of air voids: (a) Size 1; (b) Size 2; (c) Size 3; (d) Size 4.

analysis about the influences by air void contents on the low-temperature properties. Thus, the variation of air void content within the middle part has important impacts on the low-temperature property of the testing sample.

4.4. Effects by Air Void Size on Low-Temperature Property. To analyze the effects by air void size on the low-temperature property, different numbers of asphalt mortar elements contacting with each other were removed to get air voids with different sizes. During PFC3D modeling, four different air void sizes were modeled by removing mortar element (named Size 1), two interconnected mortar elements (named Size 2), three interconnected mortar elements (named Size 3), and four interconnected mortar elements (named Size 4). As shown in Figure 13, while the total air void content was kept as 4%, samples with different single air void sizes were built for virtual bending beam tests. The testing results are shown in Figure 14. It can be seen that all of the three indices decline

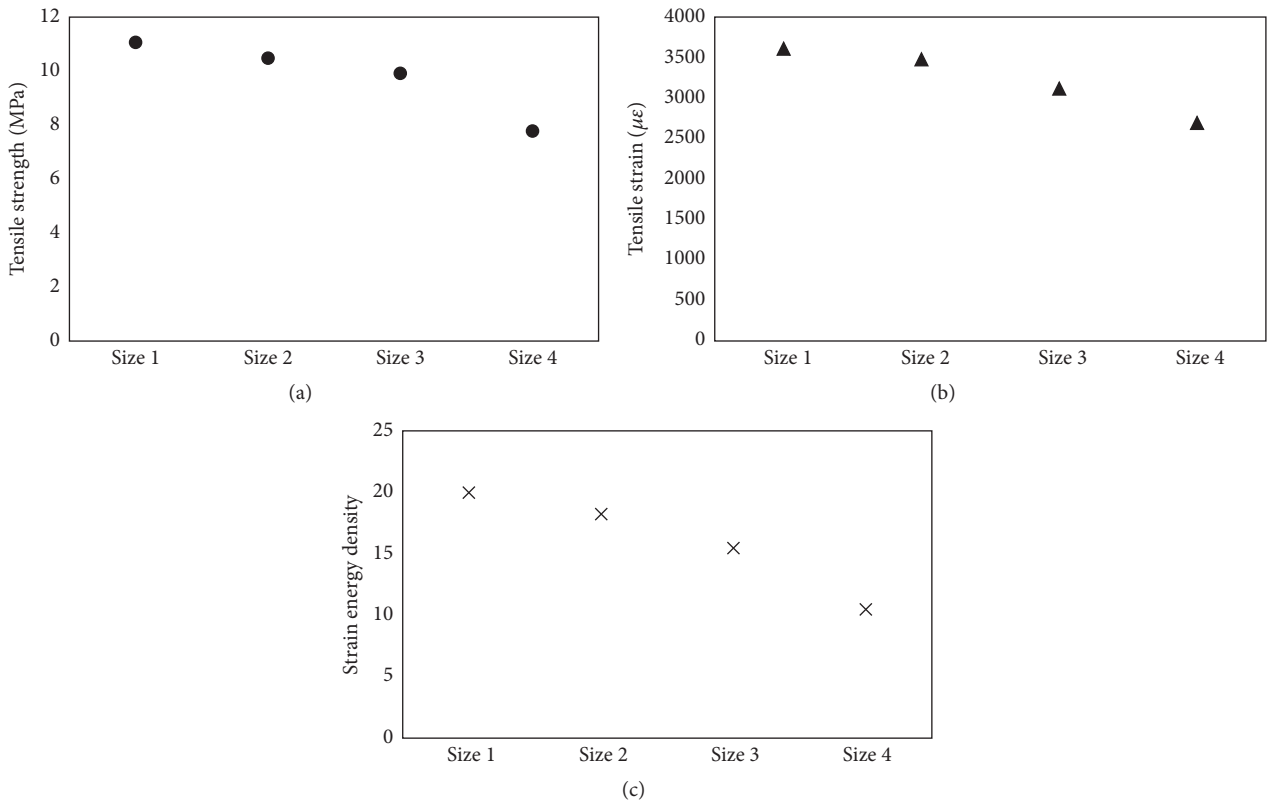

Figure 14: Effects by air void size on low-temperature property: (a) tensile stress; (b) tensile strain; (c) strain energy density.

with the air void size growing. It is shown that smaller air void size of asphalt concrete results in better low-temperature property of asphalt concrete.

5. Conclusions

Micromechanical modeling procedure based on discrete element method and PFC3D was built to simulate the low-temperature bending beam test in laboratory. Based on laboratory testing data, the validity of virtual test to characterize the low-temperature property of asphalt concrete was proved. It provides an effective method to analyze the impacts by air voids on the low-temperature properties of dense-graded asphalt concrete which are difficult to be carried out by laboratory tests.

It is proved that the growing of air void content weakens the low-temperature properties of dense-graded asphalt concrete, especially when the content of air voids is bigger than the designed content of air voids. Even with the same mix design and content of air voids, asphalt concrete can still exhibit very different low-temperature properties. Nonuniform air voids distribution and air void sizes variation have important impacts on the low-temperature properties of asphalt concrete, especially when the air void content and size within the loading area of asphalt concrete vary. Therefore, lower air void content, uniform distribution of air voids, and small size of interconnected air voids are helpful to improve the low-temperature properties of asphalt concrete.

Future study will focus on different types of asphalt concretes such as stone matrix asphalt concrete and porous asphalt concrete, different types of air voids such as impermeable void and permeable void, and the relationship between volumetric characteristics and asphalt concrete behaviors.

Competing Interests

The authors declare no competing interests regarding the publication of this paper.

Acknowledgments

The study is financially supported by the National Natural Science Foundation of China (no. 51378006), National Science and Technology Support Program (2014BAG05B04), Huoyingdong Foundation of the Ministry of Education of China (no. 141076), Excellent Young Teacher Program of Southeast University (2242015R30027), Natural Science Foundation of Jiangsu (BK20161421 and BK20140109), State Key Laboratory of High Performance Civil Engineering Materials (2014CEM008), and National Engineering Laboratory for Surface Transportation Weather Impacts Prevention (NELLM201604).

References

[1] Y. Q. Zhang, R. Luo, and R. L. Lytton, "Mechanistic modeling of fracture in asphalt mixtures under compressive loading,"

Journal of Materials in Civil Engineering, vol. 25, no. 9, pp. 1189–1197, 2013.

[2] Y. Zhang, X. Luo, R. Luo, and R. L. Lytton, "Crack initiation in asphalt mixtures under external compressive loads," *Construction and Building Materials*, vol. 72, pp. 94–103, 2014.

[3] J. Chen, H. Wang, and L. Li, "Virtual testing of asphalt mixture with two-dimensional and three-dimensional random aggregate structures," *International Journal of Pavement Engineering*, 2015.

[4] J. Chen, M. Zhang, H. Wang, and L. Li, "Evaluation of thermal conductivity of asphalt concrete with heterogeneous microstructure," *Applied Thermal Engineering*, vol. 84, pp. 368–374, 2015.

[5] H. Wang, J. Wang, and J. Q. Chen, "Micromechanical analysis of asphalt mixture fracture with adhesive and cohesive failure," *Engineering Fracture Mechanics*, vol. 132, pp. 104–119, 2014.

[6] J. P. Zhang, J. Pei, and Z. Zhang, "Development and validation of viscoelastic-damage model for three-phase permanent deformation of dense asphalt mixture," *Journal of Materials in Civil Engineering*, vol. 24, no. 7, pp. 842–850, 2012.

[7] Y. Zhang, B. Birgisson, and R. Lytton, "Weak form equation—based finite-element modeling of viscoelastic asphalt mixtures," *Journal of Materials in Civil Engineering*, vol. 28, no. 2, Article ID 04015115, pp. 1–13, 2016.

[8] Q. Dai and Z. You, "Prediction of creep stiffness of asphalt mixture with micromechanical finite-element and discrete-element models," *Journal of Engineering Mechanics*, vol. 133, no. 2, pp. 163–173, 2007.

[9] P. A. Cundall, "A computer model for simulating progressive large scale movements in blocky rock systems," in *Proceedings of the Symposium of International Society of Rock Mechanics*, vol. 1, pp. 2–8, Nancy, France, 1971.

[10] P. A. Cundall and O. D. L. Strack, "A discrete numerical model for granular assemblies," *Géotechnique*, vol. 29, no. 1, pp. 47–65, 1979.

[11] W. G. Buttlar and Z. P. You, "Discrete element modeling of asphalt concrete: a micro-fabric approach," *Transportation Research Record*, vol. 1757, pp. 111–118, 2001.

[12] A. Abbas, E. Masad, T. Papagiannakis, and T. Harman, "Micromechanical modeling of the viscoelastic behavior of asphalt mixtures using the discrete-element method," *International Journal of Geomechanics*, vol. 7, no. 2, pp. 131–139, 2007.

[13] Y. Liu and Q. Dai, "Viscoelastic model for discrete element simulation of asphalt mixtures," *Journal of Engineering Mechanics*, no. 4, pp. 324–333, 2009.

[14] A. C. Collop, G. R. McDowell, and Y. Lee, "Use of the distinct element method to model the deformation behavior of an idealized asphalt mixture," *International Journal of Pavement Engineering*, vol. 5, no. 1, pp. 1–7, 2004.

[15] Z. You, S. Adhikari, and Q. Dai, "Three-dimensional discrete element models for asphalt mixtures," *Journal of Engineering Mechanics*, vol. 134, no. 12, pp. 1053–1063, 2008.

[16] M. J. Khattak and C. Roussel, "Micromechanical modeling of hot-mix asphalt mixtures by imaging and discrete element methods," *Transportation Research Record*, no. 2127, pp. 98–106, 2009.

[17] M. J. Khattak, A. Khattab, H. R. Rizvi, S. Das, and M. R. Bhuyan, "Imaged-based discrete element modeling of hot mix asphalt mixtures," *Materials and Structures*, no. 48, pp. 2417–2430, 2015.

[18] D. Zhang, X. Huang, and Y. Zhao, "Algorithms for generating three-dimensional aggregates and asphalt mixture samples by the discrete-element method," *Journal of Computing in Civil Engineering*, vol. 27, no. 2, pp. 111–117, 2013.

[19] S. Hou, D. Zhang, X. Huang, and Y. Zhao, "Investigation of micro-mechanical response of asphalt mixtures by a three-dimensional discrete element model," *Journal of Wuhan University of Technology: Materials Science Edition*, vol. 30, no. 2, pp. 338–343, 2015.

[20] W. G. Buttlar, H. Kim, and M. P. Wagoner, "Toward realistic heterogeneous fracture modeling of asphalt mixture using disk-shaped compact tension test based on discontinuum approach," in *Proceedings of the CD-ROM of the Transportation Research Board 85th Annual Meeting*, no. 06-2975, pp. 1–23, Washington, DC, USA, 2006.

[21] H. Kim, M. P. Wagoner, and W. G. Buttlar, "Micromechanical fracture modeling of asphalt concrete using a single-edge notched beam test," *Materials and Structures*, vol. 42, article 677, 2009.

[22] H. Kim and W. G. Buttlar, "Discrete fracture modeling of asphalt concrete," *International Journal of Solids and Structures*, vol. 46, no. 13, pp. 2593–2604, 2009.

[23] H. Kim and W. G. Buttlar, "Multi-scale fracture modeling of asphalt composite structures," *Composites Science and Technology*, vol. 69, no. 2, pp. 2716–2723, 2009.

[24] X. Yang, Q. Dai, Z. You, and Z. Wang, "Integrated experimental-numerical approach for estimating asphalt mixture induction healing level through discrete element modeling of a single-edge notched beam test," *Journal of Materials in Civil Engineering*, vol. 27, no. 9, Article ID 04014259, 2008.

[25] J. Chen, T. Pan, and X. Huang, "Discrete element modeling of asphalt concrete cracking using a user-defined three-dimensional micromechanical approach," *Journal of Wuhan University of Technology: Materials Science Edition*, vol. 26, no. 6, pp. 1215–1221, 2011.

[26] J. Chen, T. Pan, J. Chen, X. Huang, and Y. Lu, "Predicting the dynamic behavior of asphalt concrete using three-dimensional discrete element method," *Journal of Wuhan University of Technology-Materials Science Edition*, vol. 27, no. 2, pp. 382–388, 2012.

[27] Itasca Consulting Group, *PFC3D Version 4.0*, Itasca Consulting Group, Minneapolis, Minn, USA, 2008.